PTW Rider Injury Mechanisms from Full-Scale Crash Testing Using PMHS

John Bolte IV, Jolyon Carroll, Mara Van Meter, Angela Tesny, Daniel Meringolo,
Erin Higinbotham, Shiyang Meng, Yun-Seok Kang, Amanda Agnew

Abstract Powered Two-Wheeler (PTW) fatalities are the leading contributor among all road user deaths (WHO 2023). Recent studies documenting injuries among PTW riders rely on police reports and eyewitness accounts or retrospective crash investigator inference. This study aimed to investigate mechanisms of serious injuries in PTW-to-vehicle crash tests involving post-mortem human subjects (PMHS). Three full-scale crash tests were conducted involving a stationary 2011 Honda Accord positioned at a 30° angle from perpendicular. The vehicle was struck on its right front door by a 2022 KTM 390 Duke PTW traveling at 50 km/h, ridden by a 50th percentile male PMHS. The PMHS were equipped with six degree-of-freedom (6DOF) motion sensors placed on the sternum, nasal bone, C4, C6, T4, T12, S1, and the right and left humeri, femora, and iliac wings. Strain gages were attached to the head, thoracic cage, sternum, cervical spine, pubic rami, and throughout the upper and lower extremities. All injuries identified at post-test dissection were assigned AIS codes by a certified specialist. All data were analyzed to understand interactions between the PMHS, the PTW, and the vehicle. Strain and strain rate were used to precisely identify fracture timing, while kinematic data helped determine the mechanisms of all serious injuries. Motion tracking analysis, 6DOF data, and deformation measurements of both the vehicle and the PTW revealed consistent patterns across all tests. Each test resulted in severe injuries to the pelvis, thoracic spine, and thoracic cage, leading to comparable Injury Severity Scores (ISS). Additional serious injuries were observed in some tests, including fractures to the humerus, femur, and cervical spine. All three PMHS sustained a complete disruption of the posterior arch of the pelvis due to the occupant sliding forward into the fuel tank upon the PTW's impact with the vehicle. Anterior rib fractures were attributed to contact with the A-pillar and roof rail, while numerous posterior rib fractures resulted from inertial loading as the PMHS was propelled into the vehicle's side. Thoracic spine fractures were found to result from extension and twisting of the thoracic spine as the PMHS transitioned from the PTW to the car-side contact. The injuries observed in the full-scale crash tests were consistent with real-world injuries recently reported in the literature. Data analysis showed that the serious injuries common across the PMHS tests shared similar mechanisms of injury. Identifying these mechanisms enables the development and execution of component tests to improve the biofidelity of safety tools and establish injury assessment reference values. These enhanced safety tools can then be utilized to evaluate safety equipment designed to reduce the occurrence of such serious injuries.

Keywords Injury Mechanisms, Pelvic Injury, Post-Mortem Human Subjects (PMHS), Powered Two-Wheelers (PTW), Thoracic Injury, Thoracic Spinal Injury

I. INTRODUCTION

Motorcycles, while offering exhilarating experiences and efficient transportation, come with inherent risks. Despite advances in safety technology and awareness campaigns, motorcycle crashes continue to pose significant threats to riders, often resulting in serious injuries and fatalities. Globally, millions of individuals rely on powered two-wheelers (PTW) for transportation [1–2]. In the United States alone, registrations for motorcycles exceeded 8.6 million in 2021 [3], while Europe boasted over 39 million motorcycles and scooters on its roads in 2019 [2]. In December 2023 the World Health Organization (WHO) released the global status report on road safety and revealed that fatalities on powered two- and three wheelers (PTW) accounted for 30% of all road fatalities, putting it ahead of occupants in four-wheel vehicles (25%) and pedestrians (21%). In the region of the Americas, PTW fatalities accounted for 25% of all road user fatalities, up from 23% in the 2018 global status report [4–5]. According to the 2021 NHTSA Traffic Safety Facts 5,932 motorcyclists were killed, which is an 8% increase from 2020 and accounted for 14% of all traffic fatalities in the United States. Another 82,686 motorcyclists were injured in 2021, which is a 5% increase from the prior year. When comparing across vehicle miles traveled in 2021, the

J. Bolte IV (e-mail: john.bolte@injurybiomechglobal.org; tel: 1-614-746-1975) is President of Injury Biomechanics Global Inc. J. Carroll and S. Meng are affiliated with Autoliv in Sweden. M. Van Meter is affiliated with the Transportation Research Center Inc. A. Tesny is affiliated with the Vehicle Research and Test Center (NHTSA). D. Meringolo, Y-S. Kang, and A. Agnew are affiliated with the Injury Biomechanics Research Center at Ohio State University. E. Higinbotham is affiliated with 830 Engineering Group LLC and is a Motorcycle Crash Reconstruction Expert.

fatality rate for motorcyclists was 24 times higher than the passenger car occupant fatality rate [6].

Across recent literature, serious and fatal PTW injuries are consistently concentrated within a limited number of recurring crash configurations, rather than being broadly distributed across all crash types. The most dominant and consistently identified configuration is a frontal PTW impact into the side of another vehicle, particularly in intersection and crossing-path scenarios. Analyses of in-depth crash data from Germany, India, and China demonstrate that passenger cars are among the most common collision partners, with PTW frontal engagement into the front or side of another vehicle emerging as the most frequent configuration associated with severe injury outcomes [7]. Similarly, urban crash investigations reported that nearly half of serious PTW crashes involved head-on-side impacts, with the PTW striking the opposing vehicle using its frontal structure in many cases [8]. These findings are reinforced by European scenario development efforts, which consistently identify PTW frontal-to-vehicle side impacts as both highly prevalent (~20% of crashes) and highly injurious, forming the foundation of representative crash scenario sets [9–10].

When both crash frequency and injury severity are considered, frontal PTW-to-vehicle side impacts remain the most critical configuration for injury mitigation. Severity-weighted analyses demonstrate that these scenarios not only occur frequently but also contribute disproportionately to serious and fatal injuries due to direct loading of the rider's head and thorax during primary impact and subsequent contact with vehicle structures [7][9]. Although collision speed is not always explicitly reported, it is inherently reflected in injury severity metrics, with these configurations often involving sufficient energy transfer to produce severe outcomes. Importantly, even in urban environments where speeds may be moderate, unfavorable rider kinematics and direct interaction with rigid vehicle structures, such as doors, A-pillars, and windshields, result in a high risk of serious injury [8]. Collectively, the literature supports prioritizing frontal PTW impacts into the side of another vehicle as the single most important crash configuration for the development of targeted countermeasures and test procedures aimed at reducing serious and fatal injuries.

Epidemiology of PTW injuries demonstrates a consistent distinction between overall injury frequency and the distribution of serious and fatal outcomes. Across multiple studies, lower-extremity injuries are the most frequently observed injuries among motorcyclists, with fractures of the tibia and femur contributing substantially to overall injury burden [11–12]. Upper-extremity injuries are also common, while injuries to the head and trunk occur less frequently in absolute terms but are disproportionately represented in severe and fatal cases. This pattern is consistently observed across trauma registries, in-depth crash investigations, and fatality studies, highlighting that injury frequency alone does not reflect clinical severity [13].

When focusing specifically on serious and fatal injuries, the head and thorax emerge as the most frequently involved body regions. Head injury remains the leading cause of death in PTW crashes, with high rates of intracranial injury reported across fatal cases [14][12]. Thoracic injuries, including rib fractures and associated internal organ trauma, are also highly prevalent among severely injured riders and are frequently identified as a primary contributor to morbidity and mortality [11]. In contrast, while lower-extremity injuries dominate the overall case count, they are less frequently associated with fatal outcomes. Spinal injuries, particularly involving the thoracic and cervical regions, also occur with notable frequency in severe crashes and contribute to the overall burden of serious injury [13].

In multi-vehicle crashes involving passenger cars, especially those occurring at intersections, injury frequency patterns remain broadly consistent with overall rider injury patterns but show an increased concentration of serious injuries in the head and thorax. As mentioned alongside their frequency, these crash types represent a substantial proportion of severe PTW injuries, with in-depth studies reporting that head-on-to-side collisions are among the most common configurations associated with serious injury [8][15]. Within these cases, the head and thorax are the most frequently and severely injured body regions, while lower-extremity injuries remain common but are less dominant in defining injury severity. Collectively, literature indicates that although extremity injuries account for the majority of injuries in PTW crashes overall, the epidemiology of serious injury is driven primarily by the frequency of head, thoracic, and, to a lesser extent, spinal trauma, particularly in collisions involving passenger vehicles.

Achieving meaningful reductions in serious and fatal injuries among PTW riders requires moving beyond broad crash classifications toward a more detailed, mechanism-based understanding of how specific crash configurations and contact sources lead to injury. The collision data is clear, PTW frontal impacts into the side of passenger vehicles is a critical configuration associated with severe thoracic and head injuries. However, current epidemiological datasets remain limited in their ability to link injury outcomes to specific contact sources. Earlier crash-based analyses similarly demonstrate that rider injury is most often caused by direct impact with the opposing vehicle, but also significantly influenced by interactions with motorcycle components such as the handlebar, fuel tank, and fork assembly. Collectively, these findings underscore the need for improved, integrated datasets that connect injury patterns with detailed crash characteristics and clearly identified injury sources. Addressing these gaps will require the development of new test methodologies and boundary conditions that better replicate real-world impact conditions [16].

The objective of this study was to conduct a series of full-scale tests replicating a real-world crash scenario in which a PTW impacts the side of a passenger vehicle using an instrumented post-mortem human subject (PMHS). This configuration was selected based on in-depth accident analyses identifying head-on-to-side collisions as among the most common scenarios associated with serious injury. The resulting data will provide a foundation for improving the understanding of injury mechanisms in these crashes and are intended to support the development and validation of crash safety assessment tools. In addition, the findings may help identify body regions at elevated risk, thereby informing the design of targeted protective safety countermeasures.

II. METHODS

PMHS Characteristics

This study involved the ethical and approved use of post-mortem human subjects (PMHS) to represent 50th percentile male riders. Important factors during subject selection included the subjects' medical history, areal bone mineral density (aBMD), and any anomalies that could affect the specific study. First, a Dual-energy X-ray Absorptiometry scan (DXA) (GE Healthcare, Chicago IL) was utilized to assess lumbar spine aBMD. Subsequently, a full-body CT scan was conducted and analyzed to identify any conditions that might disqualify the subject from participation, such as spinal degeneration or trauma, prior injuries affecting targeted body regions, or other indications of conditions that might influence results (Osirix MD version 13.0.1). Table 1 presents the characteristics of the subjects and includes the statistics for all subjects and the 50th percentile male [17].

TABLE I – PMHS DEMOGRAPHICS

Subject	Sex	Age (years)	Height (cm)	Weight (kg)	BMI	aBMD L2-L4 T-Score
PTW01	M	82	178	73	23	0.7
PTW02	M	68	180	69	21	1.8
PTW03	M	75	187	73	21	2.2
Avg ± SD			182 ± 5	71 ± 3		
50th % Male		-	175	78	25.5	

General Test Information

For this study, the chosen powered two-wheeler (PTW) was a 2022 KTM 390 Duke (Fig. 1), sourced from KTM in Austria (Mattighofen, Austria). This PTW was selected as it represents a common style of motorcycle ridden around the globe and was easily accessible for testing both in the United States and in Europe. In addition, it falls into the sport category, which was the style with the largest number of fatalities in the US in 2021 [1]. The struck vehicle for all three PMHS tests was a 2011 Honda Accord. The US Honda Accord (Fig. 1) was selected to replicate similar experiments conducted in Sweden using an anthropomorphic test device (ATD) as the occupant riding a KTM 390 Duke into a stationary European Honda Accord [18]. The helmet selected for these PMHS tests was a Bell Qualifier (Bell Helmets, Rantoul, IL) which also matched the ATD tests.

Fig. 1. 2022 KTM 390 Duke (left) and 2011 US Honda Accord (right)

Instrumentation

After careful review of recent epidemiology studies which documented injuries occurring in the real-world crashes, it was determined that instrumentation should be placed on skeletal structures located in all major body regions. Strain gages (MicroMeasurements model C4A-13-060SL-350-39P), were used to determine timing of bone fracture, and six-degree-of-freedom blocks (6DOF) (6DX, DTS, Seal Beach, CA, USA), used to define the motion of the anatomical regions of interest as the PMHS interacted with the PTW, the stationary 2011 Honda Accord, and the ground. Given the scarcity of prior research, comprehensive instrumentation schemes were applied across all body segments identified as susceptible to potential injury.

On the skull, strain gages were placed on the frontal bone, both right and left parietal bones, the occipital bone, and the mandible. Strain gages were placed on both the left and right anterior aspects of the 3rd and 5th cervical vertebrae. Within the thorax, both the manubrium and the sternal body were gaged, along with the anterior aspects of ribs 2 through 10 on both the left and right sides (3 cm from the costochondral junction), and the posterior aspect of ribs 7 through 10 on both left and right sides (4 cm from the costal angle). For the lower extremities, both left and right pubic rami, mid-shaft femora, and both proximal and distal tibiae for both the left and right lower limbs were instrumented with strain gages. Finally, strain gages were placed on both medial and distal clavicles, mid-shaft humeri, and distal radii for both right and left upper limbs. In total 55 strain gages were placed on each PMHS to help identify time of fracture and thus injury mechanisms during the event.

A 6DOF motion block was placed near the center of gravity of the head, just posterior to the nasal bone. Motion blocks were also placed along the length of the spine at C4, C6, T4, T12, and S1. The thorax included a 6DOF motion block on the sternal body, while the pelvis included a block on both left and right iliac wings. Finally, motion blocks were also placed on the mid-shaft of both humeri and the mid-shaft of both tibiae. In total, 13 DTS 6DX motion blocks were placed on each PMHS. It is important to note that the 6DOF block on the right humerus directly contacted the edge of the roof rail in all three tests and, hence, the data were not able to be recorded. The locations of all 130 channels of PMHS instrumentation are shown in Fig. 2.

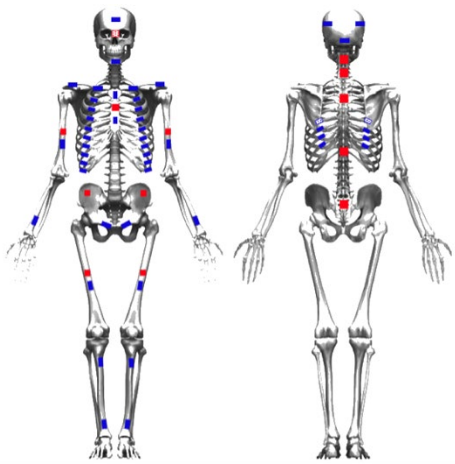

Fig. 2. PMHS Instrumentation - strain gage locations shown in blue and 6DOF locations shown in red

Once all instrumentation was placed on each PMHS, several steps were followed to ensure proper documentation of the orientation for each motion block and strain gage was known prior to the test. First, a full-body computed tomography (CT) scan with 0.6mm slice thickness was performed, and a commercial 3D CT software (Mimics, Materialize, Plymouth, MI, USA) was used to digitize locations of the 6DX block and anatomic bony landmarks. Following the CT, each PMHS was placed in a partially reclined hard chair to document the coordinates for each 6DOF block and various anatomical landmarks using a FARO EDGE arm (FARO, Lake Mary FL). Following the pre-test CT and FARO steps, each PMHS was dressed in a full-body blue morph suit.

Strain gages and 6DOF motion blocks were also applied to each KTM 390 Duke. Rosette strain gages (MicroMeasurement model CEA-06-062UR-350/P2) were placed on both left and right sides of the fuel tank and on both front forks. Subsequently, the fuel tank cover was positioned over the gages. A 6DOF block was placed at approximately the center of gravity of the KTM 390 Duke, while a 2nd 6DOF was placed on the rear aspect of the front left fork. Additionally, for PTW02 and PTW03, a 6DOF block was inserted inside the left side of each helmet near the opening for the rider's left ear.

Several camera views were used to record each crash including an onboard camera on the PTW pushcart (GoPro, San Mateo, CA, USA) and seven high-speed cameras (N3, Integrated Design Tools, Inc. Pasadena, CA, USA) located to show left overall, left quarter wide, left side down the roof rail, overhead, right overall, right quarter wide, right side down the roof rail views.

Data Acquisition and Analysis

All data were recorded using a data acquisition system (SLICE PRO, DTS, Seal Beach, CA, USA) at 20,000 Hz sampling frequency. A pressure trigger switch was placed across the front door of the Accord in line with the front tire of the impacting PTW. Contact of the KTM 390 Duke tire with the switch on the Accord was used to define time zero for each test.

A local anatomical coordinate system was defined for each skeletal element that had a 6DOF block attached to it. The three-unit vectors for each skeletal element in x-, y-, and z-directions were used to create a transformation matrix for each local anatomical coordinate system. Each 6DOF motion block coordinate system and its transformation matrix were then defined by using the digitized motion block points. The 6DOF motion block data were transformed (translation) to the origin point of each bone, and then a rotational matrix that transformed (rotation) the motion block coordinate system to the anatomical coordinate system was applied to all 6DOF data.

Following each PTW test, all videos and data were analyzed to determine the time of interest for analysis. For the injuries discussed in this article, it was determined that all critical kinematics and major injuries occurred within the first 150 msec of each crash. This period included the interaction of the PMHS with the PTW and with the Accord but is prior to the PMHS interacting with the ground. All 6DOF data were filtered using a 4th order Butterworth filter applied at numerous levels in accordance with SAE J211 guidelines [19].

Test Set-up

The PMHS was positioned on the KTM 390 Duke before the motorcycle was accelerated over 150 meters to an impact speed of 50 km/h. The PTW was secured within a custom metal propulsion cart that provided support for the motorcycle, PMHS, instrumentation cables, and onboard data acquisition system during acceleration (Fig. 3). Upon braking of the propulsion cart, the PTW and PMHS separated from the cart and continued forward unrestrained until impact with the target vehicle.

To improve test repeatability and ensure consistent impact conditions, the Honda Accord was maintained in a stationary position during testing. Finite element simulations were performed to determine the orientation of the stationary vehicle required to replicate the relative impact geometry of a real-world intersection crash scenario involving a motorcycle traveling at 50 km/h and a passenger vehicle traveling forward at 20 km/h. Based on these simulations, the Accord was positioned such that its longitudinal axis was rotated 30° from perpendicular to the motorcycle travel path, with the front of the vehicle oriented toward the approaching PTW. This configuration reproduced the relative impact angle and kinematics expected in the corresponding moving-vehicle crash scenario while maintaining highly repeatable test conditions.

It is important to note that the side mirror was removed from the vehicle for unhindered critical camera views, the gas tank was empty, and the airbags in the Accord were live and deployed by the crash event. Inch tape and photographic fiducials were placed on the Accord. Both prior to and after the crash a FARO EDGE arm (FARO, Lake Mary FL) was used to take location coordinates of the fiducials and a surface laser scan of the side of the Accord. These data were then used to calculate the amount of deformation to the Accord resulting from the crash.

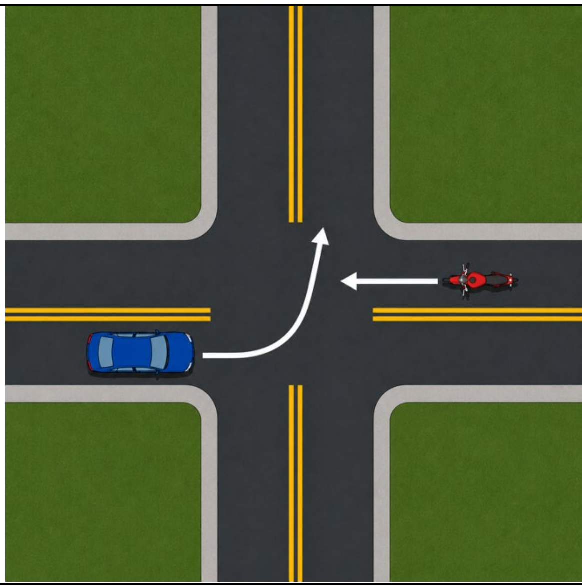

Fig. 3. Pre-Test position of the PMHS seated on the PTW and placed within the pushcart (Left) Common vehicle–PTW intersection crash configuration used for testing (right)

The PMHS was placed on the KTM 390 Duke in a repeatable manner that was selected to replicate a typical rider position. The angles of critical anatomical features from the three PMHS are shown in Table 2 and how they were measured is displayed in Appendix A. PTW2201 was seated with each of the four fingers and thumb on top of the handle grip, while the thumbs for PTW2301 and 2302 were placed beneath the grips. These changes were made to better support the upright position of the PMHs and match the typical hand position. Once seated each PMHS was suspended from the PTW through fishing line attached through skin of the scalp, upper thoracic spine, and both acromion processes of each PMHS. The fishing line was attached to cable cutter mechanisms that cut through the support line when the front tire of the PTW contacted the pressure sensor located on the door of the Accord. Following positioning, a series of radiographs were taken of each PMHS to document skeletal positions relative to the PTW. Photographic fiducials were then placed on anatomical landmarks (determined via palpation) and a FARO EDGE arm (FARO, Lake Mary FL) was used to take location coordinates of the fiducials and a surface laser scan of occupants and the KTM 390 Duke. Finally grease-based paint was applied to both the PTW and the PMHS to help visualize the interaction of both with the Honda Accord. Figure 3 shows an exemplar pre-test photo of a PMHS positioned on the PTW revealing the applied grease paint pattern and anatomical placement of fiducials.

TABLE 2 – Pre-test position measurements of each PMHS

Measurements (Deg)	**PTW 01**	**PTW 02**	**PTW 03**
Right Helmet Angle	23.5	24.7	26.5
Left Helmet Angle	23.4	26.3	27.3
Thoracic Spine Angle	12.0	11.2	12.5
Right Humerus Angle	30.0	27.0	30.7
Left Humerus Angle	32.0	27.0	28.8
Right Forearm Angle	10.0	14.5	5.8
Left Forearm Angle	10.5	17.6	6.2
Right Femur Angle	18.0	18.3	12.5
Left Femur Angle	17.0	16.0	11.6

Following the test, an additional whole-body CT was completed to assist in identifying all skeletal fractures. In addition, a detailed whole-body dissection was performed to document injuries. A Certified Abbreviated Injury Scale (AIS) Specialist (CAISS) classified all skeletal and soft tissue injuries using the AIS 2015 Dictionary [20].

III. RESULTS

The whole-body kinematics of each PMHS are shown in Appendix B. The sequential still images from an offboard camera begin at time zero, defined as initial contact between the PTW front wheel and the sedan-mounted pressure switch. Each row represents 10 ms intervals over the first 150 ms of the event.

A comprehensive summary of injuries for all three tests is provided in Table 3, including corresponding Abbreviated Injury Scale (AIS), Maximum AIS (MAIS), and Injury Severity Score (ISS) values [20]. Injury patterns were highly consistent across the three crash tests, both in terms of affected body regions and overall severity. Notably, no injuries to the head or face were identified in any PMHS, attributable to the use of helmets during testing. In contrast, three body regions demonstrated consistently severe injury outcomes across all tests: the thorax, thoracic spine, and pelvis. The focus of the remaining analysis in this paper will be on these common injuries across all three tests. Further analysis of injuries to the cervical spine, upper extremities, and lower extremities will be conducted in the future.

Within the thorax, the total number of rib fractures ranged from 17 to 22 per PMHS, involving 13 to 15 distinct ribs. In all cases, a fracture of the sternal body was also observed. Spinal injuries were present in each test, with a key finding being a major compression fracture of the T11 vertebral body in all three PMHS. In one case (PTW 03), the T11 fracture was associated with a complete spinal cord transection, classified as a critical (AIS5) injury. Finally, all tests resulted in complete disruption of the posterior pelvic arch, indicating severe loading of the pelvis during the rider–vehicle interaction.

TABLE 3 – PMHS Injury Summary

		PTW 01		PTW 02		PTW 03	
		Injury	*AIS*[1]	*Injury*	*AIS*[1]	*Injury*	*AIS*[1]
Thorax	NRF/NFR*	18/13	3	17/13	3	22/15	3
	Pneumothorax+	X	4	X	2		
	Sternal body	X	2	X	2	X	2
Upper Extremity	Scapula			L	2		
	Clavicle	R	2	R	2		
	Humerus	R	3	R	2		
	Radius			L	2		
	Ulna			R	2		
	Wrist					L/R	2
Spine	Cervical			C4	3		
				C5	3		
				C6	3	C6	3
	Thoracic			T1	3		
						T2	1
				T3	3		
		T11	3	T11	3	T11(cord)	5
	Lumbar			L1	2		
				L5	1	L5	1
Lower Extremity	Pelvis	X	4	X	4	X	4
	Femur					L/R	3
	Tibia/Fibula					L	2
Abdomen	Liver	X	2	X	2		
MAIS		**4**		**4**		**5**	
ISS		**41**		**34**		**50**	

*NRF = Number of Rib Fractures. NFR = Number of Fractured Ribs. R = Right. L = Left. X = injury occurred at this location. [1]AIS 2015 injury severities, +Pneumothorax was diagnosed by presence of a pleural laceration, small (minor) or large (major) to translate to AIS codes.

To further characterize thoracic injury patterns, Fig. 4 presents a schematic representation of the rib cage for each PMHS, with the location of all documented fractures indicated by red "×" markers. The schematics demonstrate a consistent asymmetry in fracture distribution, with a greater number of fractures occurring on the right side compared to the left, as well as a higher concentration in the superior ribs. An important finding across the test series is the presence of numerous posterior rib fractures. Posterior fractures were identified in all three PMHS and were predominantly distributed in both the upper and lower rib regions, suggesting complex loading conditions involving both direct anterior impacts and subsequent thoracic deformation due to inertial loading.

PTW 01 PTW 02 PTW 03

Fig. 4. Anterior and posterior schematics of the thoracic cage for each PMHS (Fracture= **X**)

Representative strain gage data from the anterior rib gages of one PMHS are presented in Fig. 5. Strain and strain rate histories were evaluated for each gage to determine the timing of rib fractures during the impact event. An exemplar plot using a single anterior rib gage to show how fracture timing was determined is shown in Appendix C. In this example, multiple right-side ribs exhibited fracture at approximately 111 ms, indicated by a rapid drop in measured strain. A corresponding high-speed video frame at 111 ms illustrates the PMHS kinematic position at the time of fracture. Synchronization of strain-based fracture timing with video analysis enables identification of the rider–vehicle interactions responsible for specific injuries. In this case, the timing of upper right-side rib fractures corresponds to impact of the right shoulder and upper right thorax with the upper A-pillar and leading edge of the roof rail.

Fig. 5. Exemplar strain data for right and left side anterior ribs (each line is strain from a sperate rib as shown in each legend) and a still frame showing the position of the PMHS at the onset of fracture

A fracture of the T11 vertebra was observed in all three full-scale crash tests. Post-test full-body CT images of the lower thoracic spine, Fig. 6, demonstrate a transverse fracture extending across the vertebral body in each case. Kinematic data from six-degree-of-freedom motion blocks affixed to T4 and T12 were used to quantify relative motion of the upper thoracic spine with respect to the lower thoracic region (Fig. 7). Interpretation of these data in the context of event timing indicates that the pelvis–fuel tank interaction occurs at approximately 50–60 ms, followed by contact between the upper thorax and the obliquely oriented (30° crabbed) roof rail between 95–115 ms. Between these two interaction events, the thoracic spine undergoes substantial multi-planar deformation. Across all tests, the measured kinematics indicate 30–50° of extension, combined with 10–25° of lateral bending and approximately 10° of axial rotation. These coupled motions occur as the rider transitions from pelvic loading against the fuel tank to upper body engagement with the vehicle.

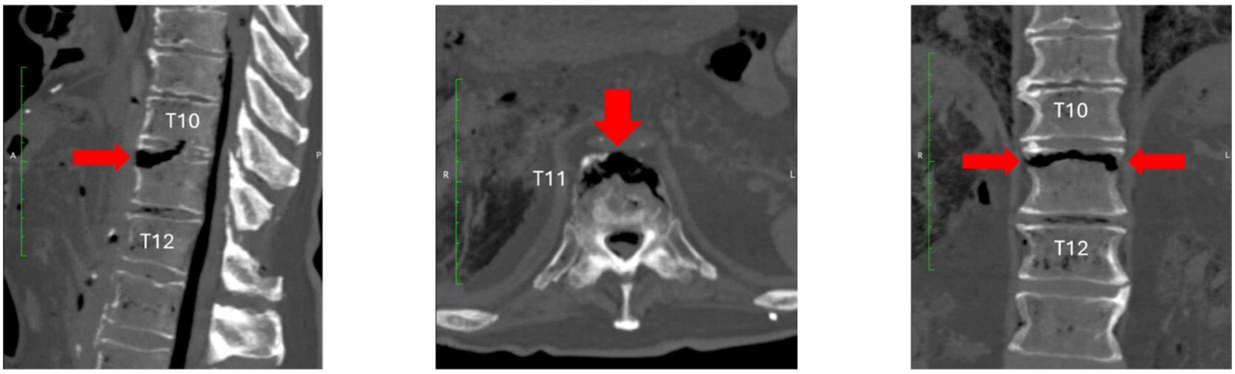

Fig. 6. Exemplar CT scan of the lower thoracic spine (left = sagittal, middle = axial, right = coronal views) following the test revealing a fracture of the T11 vertebral body (red arrows).

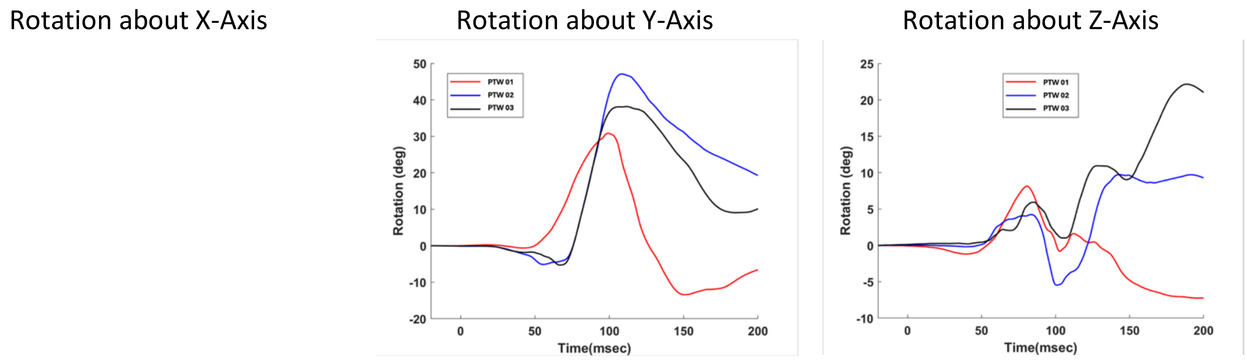

Fig. 7. Upper spine (T4) rotation with respect to the lower spine (T12).

All PMHS sustained complete disruption of the posterior pelvic ring, classified as a severe (AIS4) injury. An exemplar post-test CT image of the pelvis is shown in Fig. 8, with red arrows indicating fractures and joint separations identified during autopsy. Strain gage data from sensors placed on the bilateral superior pubic rami were used to determine the timing of anterior pelvic fractures. In the exemplar case, fracture of the pubic rami occurred at approximately 53 ms. The corresponding high-speed video frame (Fig. 8) demonstrates that, at this time, the pelvis had translated forward along the seat and engaged the fuel tank of the PTW.

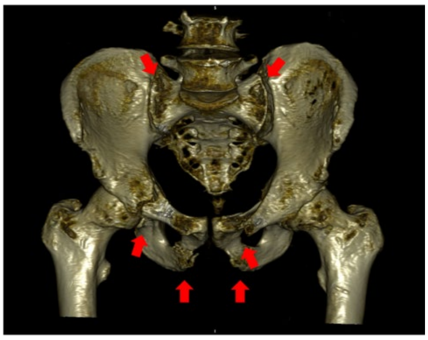

Fig. 8. Exemplar pelvis 3D CT revealing a complete disruption of the posterior arch (left), pubic ramus strain data revealing fracture timing (middle), and a still showing the timing of the pubic fracture (right)

Kinematic analysis using 6DOF motion blocks mounted on the bilateral iliac wings and sacrum was performed to evaluate pelvic motion relative to the posterior midline(Fig. 9). These data indicate that the pelvis rotated anteriorly as it translated into the fuel tank, consistent with observations from video analysis. Following fracture of the pubic rami, the iliac wings exhibited medial rotation toward the midline, indicative of a closed-book deformation pattern, which explains opposite polarities in angular velocity about the x-axis (Fig. 9).

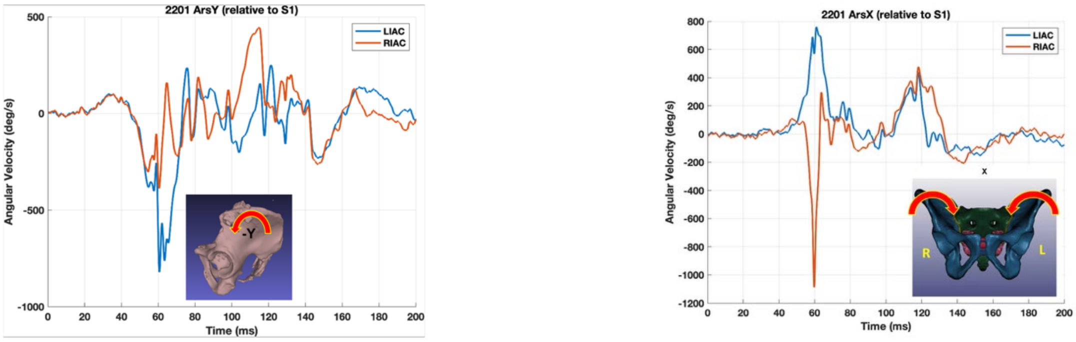

Fig. 9. Angular velocity of both right and left iliac wings with respect to the sacrum about y-axis (left) and x-axis (right)

IV. DISCUSSION

The present full-scale PMHS tests provide rare, mechanism-level evidence linking a common real-world PTW crash configuration to reproducible patterns of severe injury in the thorax, thoracic spine, and pelvis. Across all three tests, the rider kinematics were highly consistent, and each PMHS sustained severe injuries in all three regions. This repeatability is important because much of the existing PTW literature is epidemiologic or retrospective in nature and identifies injury distributions well but is less able to define the precise sequence of loading events that produce those injuries. In the current tests, the progression from forward-rider translation, to pelvis–fuel tank engagement, to upper body interaction with the A-pillar and roof rail provides a coherent explanation for the combined injury pattern observed.

Kinematics

As shown in Appendix A, the whole-body kinematics of the PMHS were highly consistent across all three crash tests up to and throughout the main contact with the vehicle. During the initial 0–50 ms, the rider maintained an upright posture while translating forward along the seat toward the fuel tank. Concurrently, the PTW front tire compressed against the side of the sedan, inducing a leftward rotation of the front tire and handlebars. At approximately 50–60 ms, the anterior pelvis of each PMHS engaged and compressed into the fuel tank, producing consistent tank deformations across all tests. As the pelvis and lower extremities decelerated due to this interaction, the upper body continued its forward motion, resulting in spinal extension between 50–70 ms.

Due to the 30° oblique orientation of the sedan relative to the PTW and a pure perpendicular crash, the rider's right upper extremity was the first body region to contact the vehicle, impacting the right front window at approximately 60–70 ms and resulting in window fracture in two of the three tests. The riders then translated up and over the fuel tank, with the right shoulder and right anterior thorax serving as the initial torso contact points with the vehicle between 70–100 ms.

In all tests, the right anterior thorax and shoulder subsequently impacted the upper A-pillar and leading edge of the roof rail. Continued forward momentum and rotation of the upper body led to secondary contact of the sternum, left anterior thorax, and left shoulder with the roof rail between 90–120 ms. Finally, the head and helmet contacted the roof structure between 120–150 ms. Post-impact trajectories varied slightly: two PMHS came to rest on the ground adjacent to the vehicles, while the third came to rest on the roof of the sedan.

Thoracic Injuries

The thoracic findings of the present study are strongly supported by the broader literature, which consistently identifies the chest as one of the most important body regions in serious and fatal PTW trauma. In the German in-depth analysis by Gidion *et al.*, rib cage fracture was the most frequent AIS3+ thoracic injury and thoracic injury was among the highest priorities for PTW injury prevention, especially in impacts with passenger cars [11]. Similarly, Piantini *et al.* reported that the head and thorax were the most seriously injured body regions in serious urban PTW-versus-other-vehicle crashes, with head-on-side collisions being the dominant severe crash configuration [8]. Older mortality-focused work also supports the clinical importance of the thorax, showing that chest trauma, including rib fractures, lung injury, hemothorax, and major vascular injury, is closely associated with fatal outcome after motorcycle crashes [14].

These PMHS tests add a more specific mechanical interpretation of how these thoracic injuries occur in a PTW frontal impact into the side of a passenger vehicle. The data indicate that anterior rib fractures were associated with direct loading of the anterior thorax against the leading edge of the roof rail, while the numerous posterior rib fractures appear to reflect secondary thoracic deformation produced by continued upper-body momentum and inertial loading after primary torso contact. This distinction is important and is supported by the fracture timing, as strain gauge measurements demonstrated that posterior rib fractures occurred later in the event. The literature has often treated thoracic injury as produced by a single uniform impact, but these data reveal it is the result of combined local compression from stiff vehicle structures and global chest deformation as the torso continues to displace into the side of the vehicle. These findings have implications for countermeasure development. If rib fractures are being generated by both direct structural contact and secondary inertial deformation, then thoracic protection systems for PTW riders will need to address not only force attenuation but also the management of torso kinematics and load distribution.

Thoracic Spine

In all tests, PMHS sustained a T11 fracture, and the instrumentation demonstrated a consistent pattern of lower thoracic multi-planar deformation between the pelvis–fuel tank interaction and upper torso engagement with the vehicle. Specifically, the lower thoracic spine underwent extension combined with lateral bending and axial rotation before fracture. This suggests that the injury mechanism is not pure extension or pure compression, but a coupled loading response arising from differential restraint of the pelvis and continued forward motion of the upper torso.

This observation is consistent with prior clinical and epidemiological studies demonstrating a high prevalence of thoracic spinal injury in motorcyclists [21]. Thoracic spine injuries have been shown to occur more frequently in motorcycle crashes than in automobile crashes, with a greater likelihood of severe or complete spinal cord injury [22]. Additionally, prior work has identified the mid- to lower-thoracic region as a common site of injury, often associated with high-energy loading and complex deformation patterns [21].

The present work advances that literature by providing a mechanical explanation for why the lower thoracic region is vulnerable in this crash mode. The rider's pelvis is abruptly loaded and slowed at the fuel tank, while the torso continues forward and upward toward the vehicle side. This creates a transient but severe mismatch in motion between the lower and upper body. In these tests, the mismatch manifested as extension, lateral bending, and rotation centered in the lower thoracic spine. That mechanism differs somewhat from simpler descriptions in prior literature that emphasize flexion-based loading, and it suggests that PTW spinal injury assessment should explicitly account for multi-planar deformation rather than relying on single-mode loading assumptions.

Pelvis

All three PMHS sustained complete disruption of the posterior pelvic ring, with early pubic ramus fracture occurring as the pelvis translated forward into the fuel tank. Kinematic analysis showed anterior pelvic rotation into the tank followed by medial rotation of the iliac wings, consistent with a closed-book pattern. These findings are strongly supported by prior literature identifying the fuel tank as a primary source of pelvic injury in motorcycle crashes. Meredith *et al*. reported that approximately 85% of pelvic injuries in PTW crashes were attributable to fuel tank contact, with increasing injury severity associated with progression from anterior ring fracture to combined anterior-posterior disruption [23]. Other studies have similarly identified pelvic ring injuries, particularly anteroposterior compression-type injuries, as clinically significant contributors to morbidity and mortality [14]. The present results extend this work by providing direct experimental evidence of the timing and mechanics of pelvic failure under realistic whole-body loading conditions. The findings reinforce that the fuel tank acts not only as a local impact surface but also as a critical driver of rider kinematics, initiating both pelvic injury and subsequent torso and spinal loading.

The main limitations of this study are the small sample size, the use of older male PMHS, and the focus on one crash configuration, one PTW, and one struck vehicle geometry. These factors limit generalizability across rider sizes, ages, motorcycles, impact severities, and vehicle shapes. There were other severe injuries identified in these tests (cervical spine, upper and lower extremity) that are documented in preparation for future analysis. In addition, while the mechanisms identified here are compelling, real-world crashes will include broader variability in pre-impact posture, braking, steering, vehicle motion, and secondary ground contact. Even so, the present work fills an important gap because it provides experimentally grounded evidence for how severe thoracic, thoracic spine, and pelvic injuries can arise in one of the most relevant PTW crash configurations identified in the epidemiologic literature.

V. CONCLUSION

Taken together, the thoracic, thoracic spine, and pelvic findings suggest that these injuries should not be interpreted as three independent outcomes. Instead, they appear to represent a linked mechanical sequence in frontal PTW-to-vehicle-side impacts. First, the rider translates forward and the pelvis engages the fuel tank, producing early pelvic fracture and abrupt deceleration of the lower body. Second, continued upper-body momentum generates multi-planar thoracic spine deformation as the torso rotates and extends over the now-slowed pelvis. Third, the chest and shoulder strike the upper vehicle side structures, producing direct rib fractures, while ongoing torso motion contributes to secondary posterior rib fractures. The thoracic injuries reflect direct structural contact plus inertial chest deformation; thoracic spine injury reflects coupled trunk kinematics generated by lower-body arrest and continued torso motion; and pelvic injury reflects localized but severe rider–motorcycle interaction at the fuel tank. In this sense, the three injury regions are biomechanically distinct but temporally and causally connected.

From a safety-tool perspective, this also helps explain why current PTW rider surrogates and simplified test methods remain limited. A test tool that reproduces thoracic contact without realistic pelvis loading, or pelvis loading without realistic upper-body continuation, may fail to reproduce the observed injury mechanisms. These data therefore support development of component and subsystem tests that preserve key whole-body boundary conditions, especially the relationship between pelvis restraint, torso excursion, and oblique contact with vehicle-side structures. The analysis is offered for reference with established contacts, kinematic behavior and even skeletal strains corresponding to a particular set of injuries. Hopefully this helps to define an ambitious capability for our safety-tools, both Anthropomorphic Test Devices (ATDs) and Human Body Models (HBMs), to represent and recreate in the future.

VI. ACKNOWLEDGEMENTS

We are grateful for the anatomical donors from The Ohio State University Body Donation Program whose selfless gifts made this research possible. Thank you to the faculty, staff, and students at the Injury Biomechanics Research Center (IBRC) at Ohio State and the staff at the Transportation Research Center Inc (TRC) for all of their support of these complicated tests.

VII. REFERENCES

[1] Insurance Institute for Highway Safety (IIHS), Highway Loss Data Institute (HLDI). (2022) Fatality facts 2020: Motorcycles and ATVs. IIHS–HLDI, Arlington, VA.

[2] Ordonez de Barraicua, M. (2023) ACEM statistical release – Registrations of motorcycles and mopeds in key European markets broadly stable during 2022. ACEM, Brussels.

[3] Teoh, E. R. (2021) Motorcycles registered in the United States, 2002–2021. Insurance Institute for Highway Safety, Arlington, VA.

[4] World Health Organisation. (2023) Global status report on road safety. World Health Organisation, Geneva, Switzerland.

[5] World Health Organisation. (2018) Global status report on road safety. World Health Organisation, Geneva, Switzerland.

[6] National Highway Traffic Safety Administration. (2023) Traffic safety facts 2021: Motorcycles. U.S. Department of Transportation, Washington, DC.

[7] Puthan, P., Lubbe, N., Shaikh, J., Sui, B., Davidsson, J. (2021) Defining crash configurations for powered two-wheelers: Comparing ISO 13232 to recent in-depth crash data from Germany, India and China. *Accident Analysis & Prevention*, **151**: p.105957.

[8] Piantini, S., Pierini, M., *et al.* (2016) Injury analysis of powered two-wheeler versus other-vehicle urban accidents. Proceedings of the International Research Council on the Biomechanics of Injury Conference, 2016, Malaga, Spain.

[9] Mensa, G., Piantini, S., *et al.* (2019) D.1.3 Guidelines for the policy making: Future trends in accident scenarios and ISO 13232 review (PIONEERS Deliverable D1.3). European Union Horizon 2020 Research and Innovation Programme, Brussels.

[10] Atalar, D., Thomas, P. (2019) Powered two-wheeler crash scenario development. *Accident Analysis & Prevention*, **125**: pp.198–206.

[11] Gidion, F., Carroll, J., Lubbe, N. (2019) Motorcyclist injuries: Analysis of German in-depth crash data to identify priorities for injury assessment and prevention. *Accident Analysis & Prevention*, **163**: p.106463.

[12] Lin, M. R., Kraus, J. F. (2009) A review of risk factors and patterns of motorcycle injuries. *Accident Analysis & Prevention*, **41**(4): pp.710–722.

[13] Wisch, M., Breunig, S., *et al.* (2019) Powered two-wheelers – Road traffic accident scenarios and common injuries (PIONEERS Deliverable D1.1). European Union Horizon 2020 Research and Innovation Programme, Brussels.

[14] Ankarath, S., Giannoudis, P. V., Barlow, I., Bellamy, M. C., Matthews, S. J., Smith, R. M. (2002) Injury patterns associated with mortality following motorcycle crashes. *Injury*, **33**: pp.473–477.

[15] Serre, T., Masson, C., Perrin, C., Martin, J.-L., Moskal, A., Llari, M. (2012) The motorcyclist impact against a light vehicle: Epidemiological, accidentological and biomechanic analysis. *Accident Analysis & Prevention*, **49**: pp.223–228.

[16] Lundin, L., Iraeus, J., Pipkorn, B. (2023) Powered two-wheeler rider thoracic impact loading in crashes with the side of passenger cars: Literature review and human body model validation. Proceedings of the International Research Council on the Biomechanics of Injury Conference, 2023, Cambridge, United Kingdom.

[17] Mertz, H. J., Jarrett, K., Moss, S., Salloum, M., Zhao, Y. (2001) The Hybrid III 10-year-old dummy. SAE Technical Paper No. 2001-22-0014. SAE International, Warrendale, PA.

[18] Carroll, J., Been, B., Burleigh, M. (2023) A novel powered two-wheeler rider dummy: Specifications and initial testing. Proceedings of the International Technical Conference on the Enhanced Safety of Vehicles, 2023, Yokohama, Japan.

[19] SAE International. (2007) Instrumentation for impact test – Part 1: Electronic instrumentation (SAE Standard J211-1). SAE International, Warrendale, PA.

[20] Association for the Advancement of Automotive Medicine. (2015) Abbreviated Injury Scale: 2015 revision. AAAM, Des Plaines, IL.

[21] Robertson, A., Giannoudis, P. V., Branfoot, T., Barlow, I., Matthews, S. J., Smith, R. M. (2002) Spinal injuries in motorcycle crashes: Patterns and outcomes. *Journal of Trauma*, **53**: pp.5–8.

[22] Medina, O., Singla, V., Liu, C., Fukunaga, D., Rolfe, K. (2020) Patterns of spinal cord injury in automobiles versus motorcycles and bicycles. *Spinal Cord Series and Cases*, **6**: p.75.
[23] Meredith, L., Baldock, M., *et al.* (2016) Motorcycle fuel tanks and pelvic fractures: A motorcycle fuel tank syndrome. *Traffic Injury Prevention*, **17**(6): pp.644–649.

VIII. APPENDIX

Appendix A – Exemplar pre-test photo displaying angles recorded for PMHS positioning

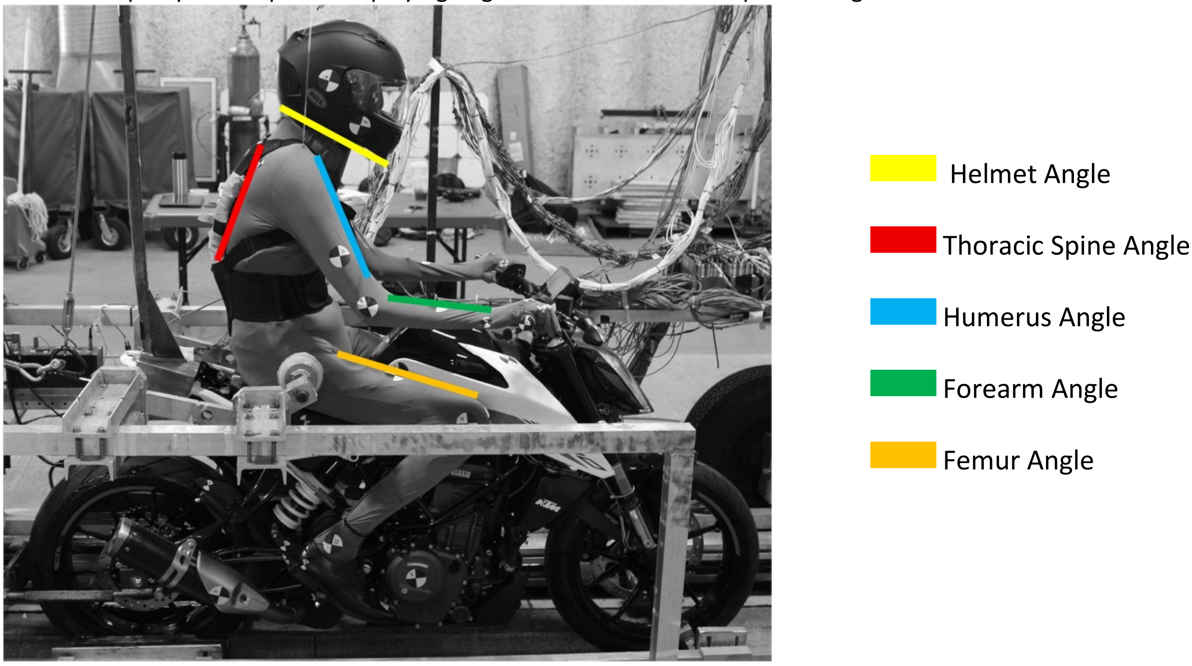

Appendix B – Still frames from the high-speed video of all 3 tests at 10 msec increments

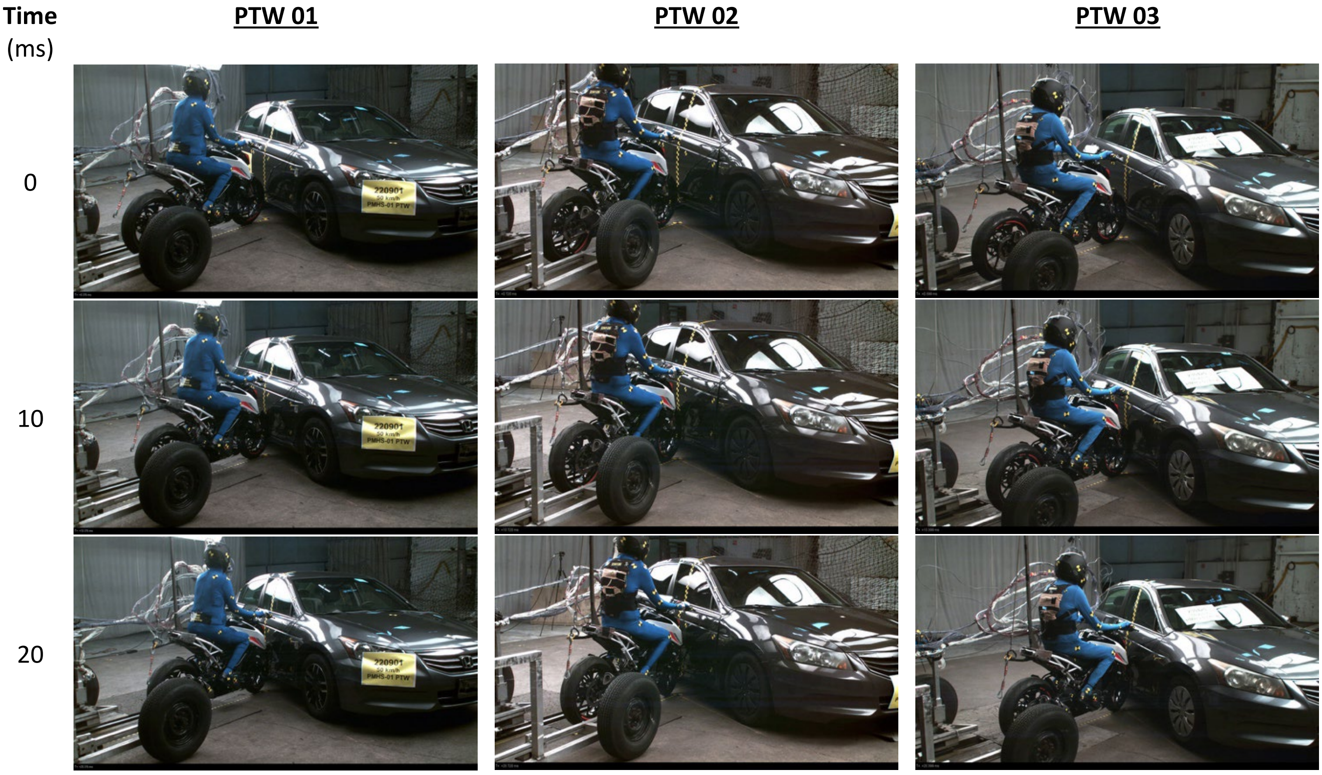

30

40

50

60

70

80

90

100

110
120
130
140
150

Appendix C – Exemplar rib strain gage plot showing both strain and strain rate with a fracture at 102 msecs